European Journal of Medicinal Chemistry 46 (2011) 6015–6024

Contents lists available at SciVerse ScienceDirect

European Journal of Medicinal Chemistry

journal homepage: http://www.elsevier.com/locate/ejmech

Original article

One-pot synthesis and biological evaluation of 2-pyrrolidinyl-4-amino-5-(3′,4′,5′-trimethoxybenzoyl)thiazole: A unique, highly active antimicrotubule agent

Romeo Romagnoli [a,*], Pier Giovanni Baraldi [a], Carlota Lopez Cara [a], Maria Kimatrai Salvador [a], Roberta Bortolozzi [b], Giuseppe Basso [b], Giampietro Viola [b,**], Jan Balzarini [c], Andrea Brancale [d], Xian-Hua Fu [e], Jun Li [e], Su-Zhan Zhang [e,***], Ernest Hamel [f]

[a] Dipartimento di Scienze Farmaceutiche, Università di Ferrara, Via Fossato di Mortara 17-19, 44121 Ferrara, Italy
[b] Dipartimento di Pediatria, Laboratorio di Oncoematologia, Università di Padova, 35131 Padova, Italy
[c] Rega Institute for Medical Research, Laboratory of Virology and Chemotherapy, B-3000 Leuven, Belgium
[d] The Welsh School of Pharmacy, Cardiff University, CF10 3NB Cardiff, UK
[e] Cancer Institute, Key Laboratory of Cancer Prevention and Intervention, China National Ministry of Education, The Second Affiliated Hospital, School of Medicine, Zhejiang University, Hangzhou, Zhejiang Province 310009, People's Republic of China
[f] Screening Technologies Branch, Developmental Therapeutics Program, Division of Cancer Treatment and Diagnosis, National Cancer Institute at Frederick, National Institutes of Health, Frederick, MD 21702, USA

ARTICLE INFO

Article history:
Received 8 August 2011
Received in revised form
4 October 2011
Accepted 6 October 2011
Available online 15 October 2011

Keywords:
Microtubules
Structure-activity relationship
Thiazole
In vivo and *in vitro* activity
Tubulin

ABSTRACT

A wide variety of small molecules with diverse molecular scaffolds inhibit microtubule formation. In this article we report a one-pot procedure for the preparation of a novel 2-(*N*-pyrrolidinyl)-4-amino-5-(3′,4′,5′-trimethoxybenzoyl)thiazole in which the size of the substituent at the C-2 position of the thiazole ring plays an essential role in compound activity. The most active agent (**3f**) inhibited at submicromolar concentrations the growth of tumor cell lines. It also inhibited tubulin polymerization with an activity quantitatively similar to that of **CA-4**, and treatment of HeLa cells resulted in their arrest at the G2-M phase of the cell cycle. Furthermore, **3f** was effective against multidrug resistant cancer cells and inhibited the growth of the HT-29 xenograft in a nude mouse model. This indicated that **3f** is a promising new antimitotic agent with encouraging preclinical potential.

1. Introduction

Antimitotic agents are one of the major classes of cytotoxic drugs for cancer treatment, and tubulin is the target for numerous small natural and synthetic molecules that inhibit the formation of the mitotic spindle [1]. Besides mitosis, the microtubule system of eukaryotic cells is a critical element in a variety of essential cellular processes, including formation and maintenance of cell shape, regulation of motility, cell signaling, secretion and intracellular transport [2]. Among the microtubule depolymerizing agents, combretastatin A-4 (**CA-4**, **1**; Chart 1) [3], isolated from the bark of the South African tree *Combretum caffrum*, is one of the well-known natural tubulin-binding molecules affecting microtubule dynamics by binding to the colchicine site on tubulin [4]. Because of its simple structure, a wide number of **CA-4** analogs have been developed and evaluated in structure-activity relationships (SAR) studies [5].

Among the synthetic inhibitors of tubulin polymerization, we have recently described a series of 2-arylamino-4-amino-5-aroylthiazoles with general structure **2** that showed strong antiproliferative activity against tumor cell lines and inhibited tubulin polymerization by interfering with the colchicine site [6]. These compounds also caused cancer cells to arrest in the G2-M phase of the cell cycle, and all possessed a 4-aminothiazole nucleus in which substitution either at the C-2 or C-5 position played an essential role in potency.

As a part of our continuing search for novel antimitotic agents, these findings prompted us to synthesize by a one-pot four-step procedure a new series of 2-alkylamino-4-amino-5-aroylthiazole derivatives with general structure **3** in which the 2-anilino

* Corresponding author. Tel.: +39 (0) 532 455303; fax: +39 (0) 532 455953.
** Corresponding author. Tel.: +39 (0) 49 8211451; fax: +39 (0) 49 8211462.
*** Corresponding author. Tel.: +86 571 8731 5002; fax: +86 571 8702 2776.
E-mail addresses: rmr@unife.it (R. Romagnoli), giampietro.viola1@unipd.it (G. Viola), zhangsirhao@gmail.com (S.-Z. Zhang).

0223-5234/$ – see front matter © 2011 Elsevier Masson SAS. All rights reserved.
doi:10.1016/j.ejmech.2011.10.013

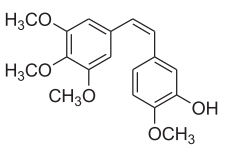

Combretastatin A-4 (CA-4), **1**

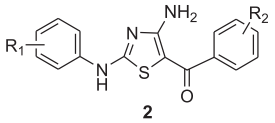

R_1=H, F, Cl, Me and OMe
R_2=H, OMe, Cl, Br and NO_2

2

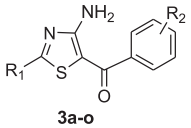

3a-o

3a, R_1=NH_2, R_2=3',4',5'-$(OCH_3)_3$
3b, R_1=$N(CH_3)_2$, R_2=3',4',5'-$(OCH_3)_3$
3c, R_1=$N(C_2H_5)_2$, R_2=3',4',5'-$(OCH_3)_3$
3d, R_1=$NCH_3(n\text{-}C_4H_9)$, R_2=3',4',5'-$(OCH_3)_3$
3e, R_1=$NCH_3(CH_2C_6H_5)$, R_2=3',4',5'-$(OCH_3)_3$
3f, R_1=pyrrolidin-1-yl, R_2=3',4',5'-$(OCH_3)_3$
3g, R_1=piperidin-1-yl, R_2=3',4',5'-$(OCH_3)_3$
3h, R_1=morpholin-4-yl, R_2=3',4',5'-$(OCH_3)_3$
3i, R_1=pyrrolidin-1-yl, R_2=3',4'-$(OCH_3)_2$
3j, R_1=pyrrolidin-1-yl, R_2=4'-OCH_3
3k, R_1=pyrrolidin-1-yl, R_2=3'-OCH_3
3l, R_1=pyrrolidin-1-yl, R_2=2'-OCH_3
3m, R_1=pyrrolidin-1-yl, R_2=4'-Cl
3n, R_1=pyrrolidin-1-yl, R_2=4'-Br
3o, R_1=pyrrolidin-1-yl, R_2=H

Chart 1. Inhibitors of Tubulin Polymerization.

moiety of compounds **2** was replaced by an amino moiety or various cyclic or acyclic alkyl amino substituents. SAR between the substitutions at the C-2 and C-5 positions of the thiazole core were evaluated.

Since it is well known that the trimethoxyphenyl group is the characteristic structural requirement to maximize the potent activity in a large series of inhibitors of tubulin polymerization, such as colchicine, **CA-4** and podophyllotoxin [7], we prepared compounds **3a**–**h**, all of which retain the 3′,4′,5′-trimethoxybenzoyl group at the C-5 position of the thiazole ring, allowing us to evaluate the effect of substitution at the C-2 position by cyclic and acyclic alkyl amines. The pyrrolidin-1-yl substituent (**3f**) resulted in a compound that was superior to the others. The potent activity of **3f** led us to synthesize a second series of derivatives **3i**–**o** in which we maintained the pyrrolidin-1-yl group at the C-2 position, but replaced the 5-(3′,4′,5′-trimethoxybenzoyl) moiety of **3f** with other benzoyl groups.

2. Chemistry

The effectiveness of the methylsulfanyl group as a leaving group was employed for the preparation of compounds **3a**–**c**, obtained by the condensation of the appropriate volatile amine with 2-methylsulfanyl-4-amino-5-(3′,4′,5′-trimethoxybenzoyl)thiazole **5** (Scheme 1). This latter derivative was obtained by a one-pot three-step sequential procedure, starting from the condensation of dimethyl cyanodithioimidocarbonate **4** and sodium sulfide, followed by the addition of 1-(3′,4′,5′-trimethoxyphenyl)-2-bromoethanone and cyclization with potassium carbonate (Scheme 1) [8]. Compounds **3d**–**o** were prepared by one-pot four step procedure from **4**, which was condensed successively with the appropriate secondary amine, sodium sulfide, the corresponding α-bromoacetophenone and finally cyclized with potassium carbonate.

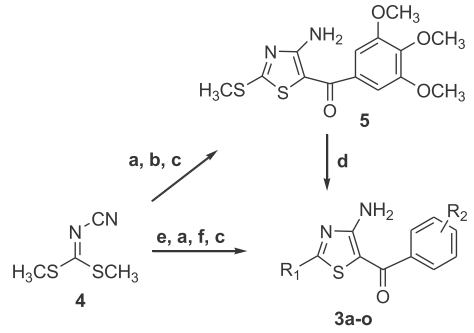

Scheme 1. *Reagents*. a: $Na_2S.9H_2O$, DMF, 70 °C, 2 h; b: 1-(3′,4′,5′-trimethoxyphenyl)-2-bromoethanone, 50 °C, 2 h; c: K_2CO_3, 1 h; d: NH_3 for **3a**, $(CH_3)_2NH$ in EtOH for **3b**, $(C_2H_5)NH$ for **3c**; e: appropriate secondary amine, DMF, 70 °C, 1 h; f: appropriate α-bromoacetophenone, 2 h, 50 °C.

3. Biological results and discussion

3.1. Antiproliferative effects of derivatives 3a–o

Table 1 summarizes the antiproliferative effects of derivatives **3a**–**o** against a panel of three human and two rodent cancer cell lines. These are murine leukemia (L1210) and mammary carcinoma (FM3A) lines and the human T-leukemia lines Molt/4 and CEM and the human cervix carcinoma HeLa line. Only **3f** showed submicromolar antiproliferative activity against all tested lines, while other derivatives generally had little activity, with IC_{50} values usually greater than 10 μM. Derivative **3f** was 10- to 100-fold less active than the reference compound **CA-4**.

Extensive exploration of SAR of this novel series of compounds showed that the presence of pyrrolidin-1-yl and 3′,4′,5′-trimethoxybenzoyl at the C-2 and C-5 positions of the 4-aminothiazole scaffold were essential for the biological activity of **3f**. Considering substitutions at the C-2 position, even minor modifications, such as expanding the pyrrolidine (**3f**) to a piperazine (**3g**) ring, caused a large reduction in antiproliferative activity.

Comparing **3f** with **3i**–**o**, all with a pyrrolidin-1-yl moiety at the C-2 position of the thiazole skeleton, demonstrated that the 3′,4′,5′-trimethoxbenzoyl moiety at the C-5 position (**3f**) was essential for activity. Its replacement with a 3′,4′-dimethoxybenzoyl (**3i**), several isomeric methoxybenzoyl (**3j**–**l**), 4′-chloro- and 4′-bromobenzoyl (derivatives **3m** and **3n**, respectively) or the unsubstituted benzoyl (**3o**) moiety all led to inactive compounds.

Conversely, when the 3′,4′,5′-trimethoxbenzoyl group was at the C-5 position of the thiazole skeleton (derivatives **3a**–**f** and **3gh**), significant loss of activity occurred upon changing the pyrrolidin-1-yl ring at the C-2 position to any other substituent that we evaluated. Alternate groups examined were the amine (**3a**), dimethylamine (**3b**), diethylamine (**3c**), *N*-methyl-*N*′-*n*-butyl amine (**3d**), *N*-methyl-*N*′-benzylamine (**3e**), piperidin-1-yl (**3g**) and morpholin-4-yl (**3h**). Thus, we speculate that the tubulin binding pocket for this portion of the molecule is quite small and allowed the presence only of the pyrrolidin-1-yl moiety.

3.2. Molecular modeling studies

This hypothesis was supported by molecular docking experiments that we performed on this series of compounds. Figure 1s (see Supplementary data) shows how compound **3f** is placed with the trimethoxyphenyl ring in proximity to Cys241, while the amino group establishes a hydrogen bond with Thr179.

Table 1
In vitro inhibitory effects of compounds **3a-o** and **CA-4**.

Compd.	IC_{50} [a](μM)				
	L1210	FM3A	Molt4	CEM	HeLa
3a	48 ± 7.2	63 ± 11	n.d.	42 ± 0.0	31 ± 6.3
3b	11 ± 2.4	12 ± 3.2	n.d.	11 ± 0.2	8.2 ± 1.1
3c	62 ± 5.4	115 ± 43	n.d	78 ± 1.7	38 ± 11
3d	53 ± 0	47 ± 0	32 ± 15	42 ± 18	31 ± 1.8
3e	>200	>200	>200	>200	>200
3f	0.37 ± 0.07	0.18 ± 0.02	0.26 ± 0.09	0.32 ± 0.04	0.34 ± 0.02
3g	43 ± 10	39 ± 16	16 ± 3.2	22 ± 12	11 ± 5.1
3h	38 ± 23	24 ± 2.2	22 ± 17	25 ± 1.3	8.8 ± 1.1
3i	60 ± 20	112 ± 38	31 ± 6.2	19 ± 1.3	36 ± 6.2
3j	>200	>200	>200	>200	>200
3k	>200	>200	>200	>200	>200
3l	>200	>200	>200	171 ± 74	185 ± 4
3m	>200	>200	>200	>200	>200
3n	>200	>200	>200	>200	>200
3o	>200	>200	>200	>200	>200
CA-4	0.003 ± 0.001	0.042 ± 0.006	0.016 ± 0.001	0.002 ± 0.001	0.002 ± 0.001

[a] IC_{50} = compound concentration required to inhibit tumor cell proliferation by 50%.

Furthermore, the pyrrolidine ring can be placed in close contact with Val181 and Met259 deep in the binding pocket.

This hydrophobic region does not seem able to accommodate more voluminous substituents, without affecting the overall binding pose of the compounds. In support of this observation, the docking results for more sterically hindered compounds, such as **3c**, **3g** and **3h**, did not produce a satisfactory binding pose (Figure 2s, Supplementary data).

3.3. *In vitro* inhibition of tubulin polymerization and colchicine binding

To further characterize the interaction with the microtubule system of this novel series of 4-aminothiazole derivatives, a selected series of compounds (**3a**–**c** and **3f**–**h**) were evaluated for their *in vitro* inhibition of tubulin polymerization. For comparison, **CA-4** was examined in contemporaneous experiments. In this assembly assay, compound **3f** was slightly less active than the reference compound **CA-4**, with IC_{50} values of 1.3 ± 0.1 and 1.0 ± 0.1 μM, respectively. In agreement with the antiproliferative data, compounds **3a**–**c** and **3g**–**h** were inactive as inhibitors of tubulin polymerization and did not inhibit tubulin assembly at concentrations as high as 20 μM.

Compound **3f** was also evaluated for inhibitory effects on the binding of [^{3}H]colchicine to tubulin. In this assay, 67% inhibition occurred with equimolar concentrations of **3f** and radiolabeled colchicine (5 μM each) in the reaction mixture. Compound **3f** was somewhat less potent than **CA-4**, which inhibited colchicine binding by 99%. These results are consistent with the conclusion that the antiproliferative activity of **3f** derives from an interaction with the colchicine site of tubulin, and this results in interference with microtubule assembly.

Because only compound **3f** had submicromolar activity as an antiproliferative agent against cancer cell lines, further evaluation was limited to this agent.

3.4. *Effects of **3f** on multidrug resistant cell lines*

Drug resistance is an important therapeutic problem caused by the emergence of tumor cells possessing different mechanisms which confer resistance against a variety of anticancer drugs [9,10]. Among the more common mechanisms are those related to the overexpression of glycoproteins capable of mediating the efflux of various drugs [9,10]. Therefore, we investigated whether **3f** inhibited the growth of two drug-resistant cell lines, one derived from a lymphoblastic leukemia ($CEM^{Vbl-100}$), the other derived from a colon carcinoma ($Lovo^{Doxo}$). Both these lines express high levels of the 170-kDa P-glycoprotein (P-gp) drug efflux pump [11,12]. As shown in Table 2, compound **3f** was equally potent toward parental cells and cells resistant to vinblastine or doxorubicin.

Resistance to microtubule inhibitors is also mediated by changes in the levels of expression of different β-tubulin isotypes and by tubulin gene mutations that result in modified tubulin with impaired polymerization properties. A-549-T12 is a cell line with an α-tubulin mutation with increased resistance to taxol [13]. Compound **3f** had greater relative activity than taxol in this cell line, suggesting that **3f** might be useful in the

Table 2
In vitro cell growth inhibitory effects of **3f** on drug resistant cell lines.

Compd.	IC_{50} [a](μM)					
	LoVo	$LoVo^{Doxo}$	CEM	CEM^{Vbl100}	A549	A549-T12
3f	0.10 ± 0.04	0.43 ± 0.19 (4.3)[b]	0.02 ± 0.006	0.01 ± 0.002 (0.2)	0.037 ± 0.013	0.16 ± 0.09 (4.3)
Doxorubicin	0.12 ± 0.03	13.1 ± 0.21 (109.6)	n.d.	n.d.	n.d.	n.d.
Vinblastine	n.d.	n.d.	0.004 ± 0.0002	0.23 ± 0.032 (56.1)	n.d.	n.d.
Taxol	n.d.	n.d.	n.d.	n.d.	0.0072 ± 0.0001	0.075 ± 0.012 (10.4)

Data are expressed as the mean ± SE from the dose–response curves of at least three independent experiments. n.d. not determined.
[a] IC_{50} = compound concentration required to inhibit tumor cell proliferation by 50%.
[b] Values in parentheses are fold resistance, indicating reduced potency of the compounds in the resistant cell lines.

treatment of drug refractory tumors resistant to other anti-tubulin drugs.

3.5. Analysis of cell cycle effects

The effects of different concentrations of compound **3f** after 24 h of treatment on cell cycle progression were examined in HeLa cells (Fig. 1, panel A). Compound **3f** caused a remarkable G2/M arrest pattern in a concentration-dependent manner, starting at 0.125 μM. In parallel we observed a concomitant decrease of cells in the G1 phase of the cell cycle (Fig. 1, panel A), while the percentage of S phase cells declined only at the highest concentration used (0.5 μM).

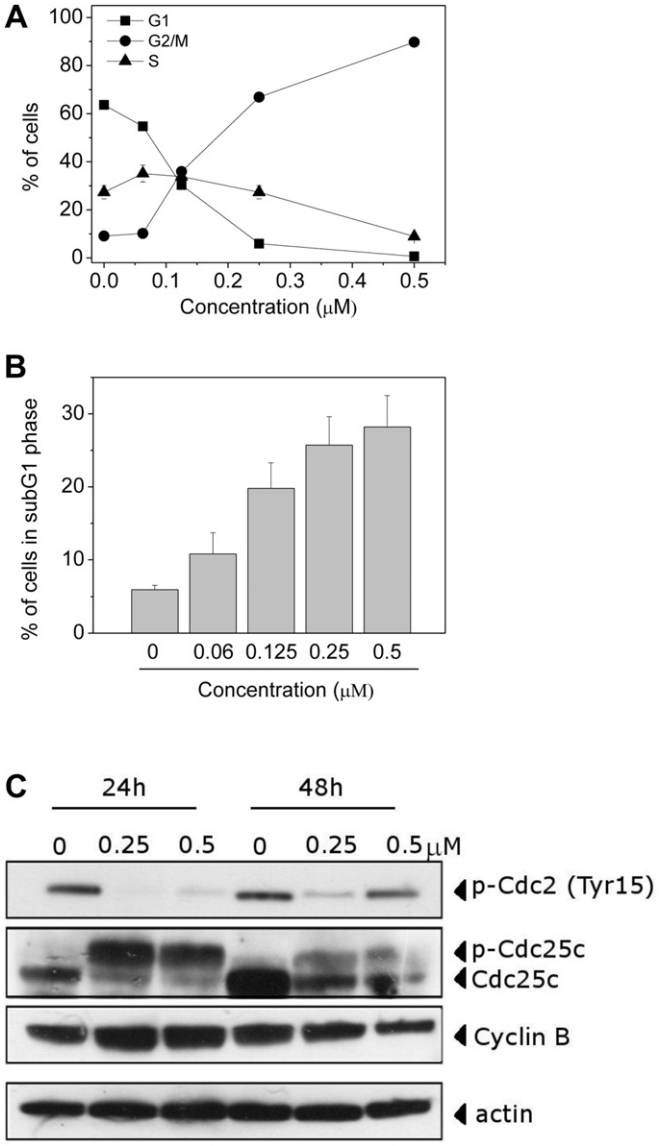

Fig. 1. Effect of compound **3f** on G2/M phase arrest in Hela cells (panel A). Cells were treated with different concentrations ranging from 0.06 to 0.5 μM for 24 h. Then the cells were fixed and stained with PI to analyze DNA content by flow cytometry. Data are presented as mean ± SEM of three independent experiments. Panel B. Percentage of cells presenting a SubG1 peak (apoptotic cells) after 24 h of treatment of HeLa cells with the indicated concentration of **3f**. Panel C. Effect of **3f** on some G2/M regulatory proteins. HeLa cells were treated for 24 or 48 h with the indicated concentration of the compound. The cells were harvested and lysed for the detection of cyclin B, p-Cdc2^{Y15} and Cdc25c expression by Western blot analysis. To ensure equal protein loading, each membrane was stripped and reprobed with anti-β-actin antibody.

More importantly, we observed a concentration-dependent increase of the cell population with a hypodiploid DNA content peak (subG1), representing those cells with a DNA content less than G1, which are usually considered to be apoptotic cells (Fig. 1, panel B). This suggests that **3f** may induce apoptosis.

We next studied the association between **3f**-induced G2/M arrest and alterations in expression of proteins that regulate cell division. Cell arrest at the prometaphase/metaphase to anaphase transition is normally regulated by the mitotic checkpoint [14]. In eukaryotic cells the activation of Cdc2 kinase is necessary for occurrence of the G2/M transition of the cell cycle. Activation of the kinase requires accumulation of the cyclin B1 protein and its dephosphorylation at Tyr15 and Thr14 [14]. As shown in Fig. 1 (panel C) in HeLa cells, **3f** caused an increase in cyclin B1 expression after 24 h of treatment that then decreased by 48 h. At the same time, there was a marked reduction in Tyr15 phosphorylation at 24 h, with partial recovery by 48 h.

In addition, slower migrating forms of phosphatase Cdc25c appeared at 24 h, followed by partial disappearance at 48 h, indicating changes in the phosphorylation state of this protein. The phosphorylation of Cdc25c directly stimulates its phosphatase activity, and this is necessary to activate Cdc2/cyclin B on entry into mitosis [14].

3.6. Compound *3f* induces apoptosis

To characterize the mode of cell death induced by **3f**, a biparametric cytofluorimetric analysis was performed using propidium iodide (PI), which stains DNA and enters only dead cells, and fluorescent immunolabeling of the protein annexin-V, which binds to phosphatidylserine (PS) in a highly selective manner [15]. Dual staining for annexin-V and with PI permits discrimination between live cells (annexin-V$^-$/PI$^-$), early apoptotic cells (annexin-V$^+$/PI$^-$), late apoptotic cells (annexin-V$^+$/PI$^+$) and necrotic cells (annexin-V$^-$/PI$^+$) [16]. As depicted in Fig. 2, compound **3f** at 24 h had already induced an accumulation of annexin-V positive cells in comparison with the control, and this accumulation was concentration-dependent, in good agreement with the appearance of the sub-G1 cells described above. After 48 h incubation, we observed a further decrease of cell viability along with a marked increase in PI positive cells.

3.7. Effect of *3f* on mitochondrial depolarization

Mitochondria play an essential role in the propagation of apoptosis [17]. It is well established that, at an early stage, apoptotic stimuli alter the mitochondrial transmembrane potential ($\Delta\psi_{mt}$). $\Delta\psi_{mt}$ was monitored by the fluorescence of the dye 5,5′,6,6′

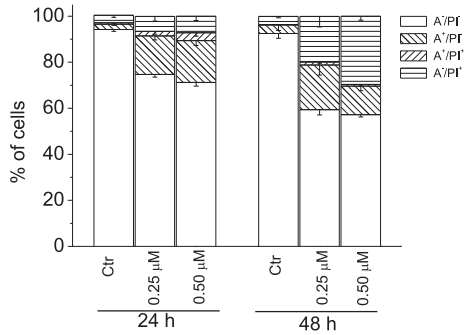

Fig. 2. Flow cytometric analysis of apoptotic cells after treatment of HeLa cells with **3f**. The cells were harvested and labeled with annexin-V-FITC and PI and analyzed by flow cytometry. Percentage of cells found in the different regions of the biparametric histograms after incubation with **3f** for 24 h or 48 h. Data are expressed as mean ± S.E.M. for four independent experiments.

tetrachlo-1,1′,3,3′-tetraethylbenzimidazol-carbocyanine (JC-1) [18]. With normal cells (high $\Delta\psi_{mt}$), JC-1 displays a red fluorescence (590 nm). This is caused by spontaneous and local formation of aggregates that are associated with a large shift in the emission. In contrast, when the mitochondrial membrane is depolarized (low $\Delta\psi_{mt}$), JC-1 forms monomers that emit at 530 nm. As shown in Fig. 3 (panel A), **3f** induced a time and concentration-dependent increase in cells with depolarized mitochondria.

Mitochondrial membrane depolarization is associated with mitochondrial production of reactive oxygen species (ROS) [19]. Therefore, we investigated whether ROS production increased after treatment with **3f**. We utilized two fluorescence indicators: hydroethidine (HE), whose fluorescence appears if ROS are generated [19a] and the dye 2,7-dichlorodihydrofluorescein diacetate (H_2-DCFDA), which is oxidized to the fluorescent compound DCF by a variety of peroxides, including hydrogen peroxide [19a].

The results presented in Fig. 3 (panels B and C) show that **3f** induced the production of large amounts of ROS in comparison with control cells, which agrees with the previously described dissipation of $\Delta\psi_{mt}$. Altogether, these results indicate that compound **3f** induced apoptosis through the mitochondrial pathway.

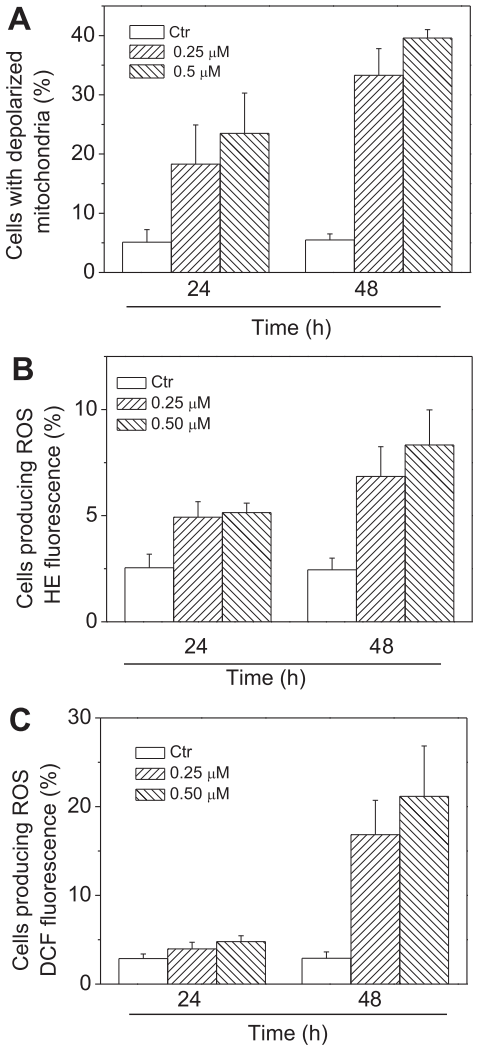

Fig. 3. Assessment of mitochondrial dysfunction after treatment with compound **3f**. Panel A. Induction of loss of mitochondrial membrane potential after 24 or 48 h of incubation of HeLa cells with compound **3f**. Cells were stained with the fluorescent probe JC-1 and analyzed by flow cytometry. Data are expressed as mean ± S.E.M. for three independent experiments. Panels B and C. Mitochondrial production of ROS in HeLa cells. After 24 or 48 h of incubation with **3f**, cells were stained with HE (panel B) or H_2-DCFDA (panel C) and analyzed by flow cytometry. Data are expressed as mean ± S.E.M. of three independent experiments.

3.8. Effect of *3f* on Bcl-2, Bax expression and caspase-3 activation

Next, we analyzed the effect of **3f** on the expression of two members of the Bcl-2 family, the anti-apoptotic Bcl-2 and the pro-apoptotic Bax. The proteins of the Bcl family play a major role in controlling apoptosis through the regulation of mitochondrial processes and the release of mitochondrial proapoptotico molecules important for the cell death pathway [20]. As shown in Fig. 4 (panel B), **3f** did not significantly affect the expression of these two proteins, except for a marked decrease at 48 h of the anti-apoptotic protein Bcl-2.

To determine if caspases were involved in **3f**-induced cell death, the expression of caspase-3 was evaluated by flow cytometry. We observed a clear activation in a time-dependent manner, of caspase-3 and cleavage of its substrate polyADP-ribose polymerase (PARP) (Fig. 4, panels A and B).

3.9. In vivo antitumor activity of compound *3f*

To evaluate the *in vivo* antitumor activity of **3f**, human colon adenocarcinoma xenografts were established by subcutaneous injection of HT-29 cells in the backs of nude mice. In preliminary experiments *in vitro*, we determined that compound **3f** showed remarkable cytotoxic activity ($IC_{50} = 0.02 \pm 0.002$ μM) against HT-

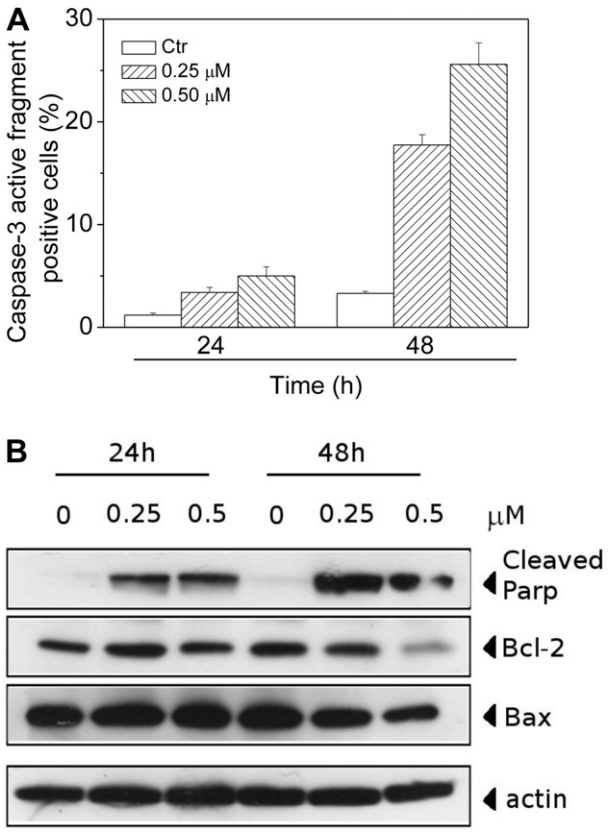

Fig. 4. Panel A. Caspase-3 induced activity by compound **3f**. HeLa cells were incubated in the presence of **3f** at the indicated concentrations. After 24 or 48 h of treatment, cells were harvested and stained with an anti-human active caspase-3 fragment monoclonal antibody conjugated with FITC. Data are expressed as percentage of caspase-3 active fragment positive cells. Panel B. Western blot analysis for the cleavage of PARP and the expression of Bcl-2 and Bax, in HeLa cells. The cell were treated with the indicated concentration of **3f** for 24 or 48 h. Whole cell lysates were subjected to SDS-PAGE, followed by blotting with the appropriate antibody or an anti-actin antibody.

29 cells, while **CA-4** showed only moderate cytotoxicity ($IC_{50} = 3.1 \pm 0.1$ μM).

Once the HT-29 xenografts reached a size of ~300 mm^3, eighteen mice were randomly assigned to one of the three groups. In two of the groups, compound **3f** or **CA-4**, prepared in DMSO, were injected intraperitoneally at doses of 100 mg/kg. All drugs, as well as a vehicle control, were administered three times a week for one week. As shown in Fig. 5, compound **3f** caused a remarkable reduction in tumor growth (58%) as compared with administration of vehicle only. The effect on tumor volume reduction by **3f** was better than that of **CA-4**, which caused a 43.7% of reduction at day 24, despite the greater antiproliferative and antitubulin activities of **CA-4**.

Although the effects of the two compounds are similar as inhibitor of tubulin polymerization, it is interesting to note that only compound **3f** exerted a statistically significant reduction of the tumor mass in comparison with the group treated with vehicle only.

During the whole treatment period, no significant weight changes occurred in the treated animals (Fig. 5, panel B). However, in the **CA-4** group two animal died on day 7 and one animal died in the **3f** on day 19. Thus, **3f** is potentially less toxic *in vivo* than **CA-4** despite equivalent or superior *in vivo* antitumor activity.

4. Conclusions

In conclusion, a series of 2-alkylamino-4-amino-5-aroylthiazoles was synthesized by a one-pot procedure. This efficient method afforded a readily accessible compound, 2-(pyrrolidinin-1-yl)-4-amino-5-(3′,4′,5′-trimethoxybenzoyl)thiazole, displaying submicromolar IC_{50} values in all cancer cell lines examined. Compound **3f** was comparable to **CA-4** as an inhibitor of tubulin polymerization through an interaction at the colchicine site. SAR studies demonstrated that an appropriate combination of C-2 and C-5 substitutions at the thiazole ring was essential for the activity. Of all substituents examined, the pyrrolidin-1-yl moiety at the C-2 position was required. These results suggested a strict spatial requirement for the substituent at the C-2 position on the thiazole scaffold at the tubulin binding site, which was confirmed in molecular docking studies. A similar phenomenon was observed with the substituent at the C-5 position, where the 3′,4′,5′-trimethoxybenzoyl moiety was the only tolerated group of all those examined and was crucial for potent biological activity.

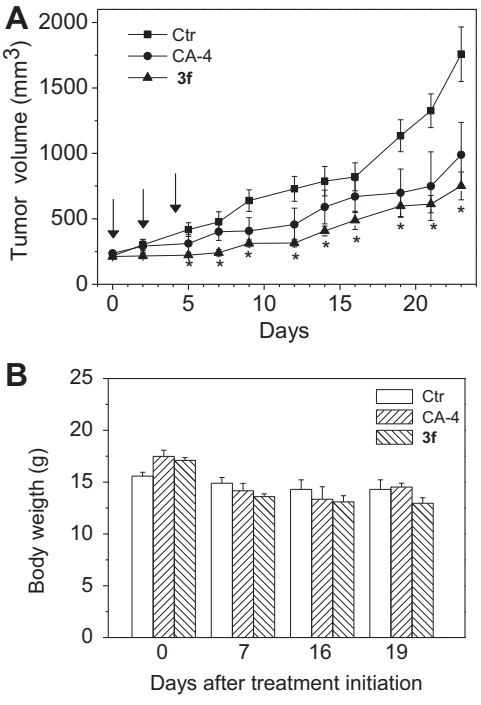

Fig. 5. Inhibition of human xenograft growth *in vivo* by compound **3f**. Panel A. HT-29 tumor-bearing nude mice were administered vehicle alone or 100 mg/kg of **3f** or **CA-4** intraperitoneally on days 0, 2 and 4 (indicated by arrows). The figure shows the tumor volume (panel A) and body weight (panel B) recorded at the indicated days after treatments. Data are expressed as mean ± SEM of tumor volume and body weight at each time point for six animals per group. $^{*}p < 0.01$ *vs.* control.

Compound **3f** was also active in suppressing the growth of drug resistant cells, and. even more importantly, it had significant *in vivo* activity in a colon cancer xenograft. These findings suggest that **3f** is a promising new antimitotic compound for the potential treatment of cancer.

5. Experimental protocols

5.1. Chemistry

5.1.1. Materials and methods

^{1}H NMR spectra were recorded on a Bruker AC 200 spectrometer. Chemical shifts (δ) are given in ppm upfield from tetramethylsilane as internal standard, and the spectra were recorded in appropriate deuterated solvents, as indicated. Positive-ion electrospray ionization (ESI) mass spectra were recorded on a double-focusing Finnigan MAT 95 instrument with BE geometry. Melting points (mp) were determined on a Buchi-Tottoli apparatus and are uncorrected. All products reported showed ^{1}H NMR spectra in agreement with the assigned structures. The purity of tested compounds was determined by combustion elemental analyses conducted by the Microanalytical Laboratory of the Chemistry Department of the University of Ferrara with a Yanagimoto MT-5 CHN recorder elemental analyzer. All tested compounds yielded data consistent with a purity of at least 95% as compared with the theoretical values. All reactions were carried out under an inert atmosphere of dry nitrogen, unless otherwise indicated. Standard syringe techniques were used for transferring dry solvents. Reaction courses and product mixtures were routinely monitored by TLC on silica gel (precoated F_{254} Merck plates), and compounds were visualized with aqueous $KMnO_4$. Flash chromatography was performed using 230–400 mesh silica gel and the indicated solvent system. Organic solutions were dried over anhydrous Na_2SO_4.

5.1.2. Synthesis of [4-amino-2-(methylsulfanyl)-1,3-thiazol-5-yl](3′,4′,5′-trimethoxyphenyl)methanone (**5**)

To a stirred suspension of $Na_2S \cdot 9H_2O$ (1.2 g, 5 mmol) in DMF (7 mL), dimethyl cyanodithioimidocarbonate **4** (730 mg, 5 mmol) dissolved in DMF (5 mL) was added, and the mixture was heated at 70 °C for 2 h. Then, 2-bromo-1-(3,4,5-trimethoxyphenyl)ethanone (2890 mg, 10 mmol) dissolved in DMF (5 mL) was slowly added dropwise at 50 °C. The mixture was heated at 50 °C for 2 h, and potassium carbonate was added (690 mg, 10 mmol). The reaction was stirred at 50 °C for 1 h more. The mixture was poured onto water (100 mL) with vigorous stirring. When a yellow precipitate appeared, the reaction mixture was filtered, and the filtrate was washed with water and dried at room temperature until a constant weight was reached. The isolated solid was purified by stirring in petroleum ether for 1 h and the mixture was filtered to afford **5** as a yellow solid. Yield. 52%, mp 130–132 °C ^{1}H NMR ($CDCl_3$) δ: 2.67 (s, 3H), 3.90 (s, 3H), 3.91 (s, 6H), 6.82 (bs, 2H), 7.03 (s, 2H). MS (ESI): $[M]^+ = 340.6$.

5.1.3. (2,4-Diamino-1,3-thiazol-5-yl)(3,4,5-trimethoxyphenyl) methanone (**3a**)

A stirred suspension of **5** (102 mg, 0.3 mmol) in a saturated solution of ammonia in absolute ethanol (10 mL) was heated in

a steel bomb for 18 h at 100 °C. After this time, the solvent was evaporated and the residue purified by column chromatography on silica gel (4% MeOH in EtOAc) to yield **3a** as a yellow solid. Yield 62%, mp 211–213 °C ^{1}H NMR (DMSO-d_6) δ: 3.42 (bs, 2H), 3.81 (s, 3H), 3.87 (s, 6H), 6.94 (s, 2H), 8.05 (bs, 2H). MS (ESI): $[M]^+ = 309.7$. Anal. calcd for $C_{13}H_{15}N_3O_4S$: C, 50.47; H, 4.89; N, 13.58; found: C, 50.23; H, 4.68; N: 13.33.

*5.1.4. [4-Amino-2-(dimethylamino)-1,3-thiazol-5-yl](3,4,5-trimethoxyphenyl)methanone (**3b**)*

A mixture of **5** (102 mg, 0.3 mmol) in a 33% solution of dimethylamine in absolute ethanol (10 mL) was heated in a steel bomb for 18 h at 100 °C. After this time, the solvent was evaporated and the residue stirred with petroleum ether. The precipitate was removed by filtration to furnish **3b** as a yellow solid. Yield 55%, mp 180–182 °C ^{1}H NMR ($CDCl_3$) δ: 2.02 (bs, 2H), 3.13 (s, 6H), 3.88 (s, 3H), 3.89 (s, 6H), 7.02 (s, 2H). MS (ESI): $[M]^+ = 337.8$. Anal. calcd for $C_{15}H_{19}N_3O_4S$: C, 53.40; H, 5.68; N, 12.45; found: C, 53.18; H, 5.46; N, 12.31.

*5.1.5. [4-Amino-2-(diethylamino)-1,3-thiazol-5-yl](3,4,5-trimethoxyphenyl)methanone (**3c**)*

The thiazole **5** (102 mg, 0.3 mmol) was added to a mixture of diethylamine (5 mL) in absolute ethanol (10 mL) and the resulting solution was heated in a steel bomb for 18 h at 100 °C. After this time, the solvent was evaporated, the residue dissolved in dichloromethane (10 mL) and the solution washed with water (5 mL) and brine (5 mL) and dried over Na_2SO_4. The solvent was removed by evaporation under reduced pressure. The residue purified by column chromatography on silica gel (40% EtOAc in petroleum ether) furnished **3c** as a brown solid. Yield 58%, mp 99–101 °C ^{1}H NMR ($CDCl_3$) δ: 1.26 (t, $J = 7.0$ Hz, 6H), 1.88 (bs, 2H), 3.53 (t, $J = 7.0$ Hz, 4H), 3.89 (s, 3H), 3.91 (s, 6H), 6.99 (s, 2H). MS (ESI): $[M]^+ = 365.7$. Anal. calcd for $C_{17}H_{23}N_3O_4S$: C, 55.87; H, 6.34; N, 11.50; found: C, 55.64; H, 6.11; N, 11.31.

*5.1.6. General procedure for the synthesis of compounds (**3d–o**)*

To a stirred solution of dimethyl cyanodithioimidocarbonate **4** (292 mg, 2 mmol) in DMF (5 mL) was added the appropriate secondary amine (2 mmol), and the mixture was heated at 70 °C for 1 h. After this time, $Na_2S{\cdot}9H_2O$ (2 mmol) was added, and the mixture was heated for 90 min at 70 °C. Then, the appropriate α-bromoacetophenone (4 mmol) dissolved in DMF (5 mL) was slowly added dropwise at 50 °C. The mixture was heated at 50 °C for 2 h, and potassium carbonate was added (276 mg, 2 mmol). The reaction was stirred at 50 °C for another 1 h. The mixture was poured onto water (20 mL) and the resulting suspension was extracted with dichloromethane (3 × 15 mL). The combined organic phases were washed with water (2 × 15 mL) and brine (20 mL), dried over Na_2SO_4 and concentrated under reduced pressure. The resulting residue was purified by stirring in ethyl ether for 1 h and filtered to furnish the final compound.

*5.1.6.1. {4-Amino-2-[butyl(methyl)amino]-1,3-thiazol-5-yl}(3,4,5-trimethoxyphenyl) methanone (**3d**).* Following the general procedure, using *N,N*-dimethylbutan-1-amine (240 μL) and 2-bromo-1-(3,4,5-trimethoxyphenyl)ethanone (1156 mg), compound **3d** was isolated as a yellow solid. Yield 72%, mp 156–158 °C ^{1}H NMR ($CDCl_3$) δ: 0.95 (t, $J = 7.2$ Hz, 3H), 1.42 (m, 2H), 1.64 (m, 2H), 2.02 (bs, 2H), 3.10 (s, 3H), 3.48 (m, 2H), 3.88 (s, 3H), 3.92 (s, 6H), 7.01 (s, 2H). MS (ESI): $[M]^+ = 379.5$. Anal. calcd for $C_{18}H_{25}N_3O_4S$: C, 56.97; H, 6.64; N, 11.07; found: C, 56.78; H, 6.43; N, 10.89.

*5.1.6.2. {4-Amino-2-[benzyl(methyl)amino]-1,3-thiazol-5-yl}(3,4,5-trimethoxyphenyl) methanone (**3e**).* Following the general procedure, using *N,N*-dimethyl(phenyl)methanamine (255 μL) and 2-bromo-1-(3,4,5-trimethoxyphenyl)ethanone (1156 mg), compound **3e** was isolated as a yellow solid. Yield 69%, mp 159–161 °C ^{1}H NMR ($CDCl_3$) δ: 2.02 (bs, 2H), 3.09 (s, 3H), 3.88 (s, 3H), 3.91 (s, 6H), 4.73. (s, 2H), 7.00 (s, 2H), 7.34 (m, 5H). MS (ESI): $[M]^+ = 413.5$. Anal. calcd for $C_{21}H_{23}N_3O_4S$: C, 61.00; H, 5.61; N, 10.16; found: C, 60.88; H, 5.47; N, 9.88.

*5.1.6.3. (4-Amino-2-pyrrolidin-1-yl-1,3-thiazol-5-yl)(3,4,5-trimethoxyphenyl)methanone (**3f**).* Following the general procedure, using pyrrolidine (170 μL) and 2-bromo-1-(3,4,5-trimethoxyphenyl)ethanone (1156 mg), compound **3f** was isolated as a yellow solid. Yield 72%, mp 228–230 °C ^{1}H NMR ($CDCl_3$) δ: 2.07 (m, 4H), 3.66 (m, 6H), 3.86 (s, 3H), 3.98 (s, 6H), 7.00 (s, 2H). MS (ESI): $[M]^+ = 363.6$. Anal. calcd for $C_{17}H_{21}N_3O_4S$: C, 56.18; H, 5.82; N, 11.56; found: C, 55.97; H, 5.61; N, 11.41.

*5.1.6.4. (4-Amino-2-piperidin-1-yl-1,3-thiazol-5-yl)(3,4,5-trimethoxyphenyl)methanone (**3g**).* Following the general procedure, using piperidine (200 μL) and 2-bromo-1-(3,4,5-trimethoxyphenyl)ethanone (1156 mg), compound **3g** was isolated as a yellow solid. Yield 74%, mp 176–178 °C ^{1}H NMR ($CDCl_3$) δ: 1.68 (m, 6H), 3.54 (m, 4H), 3.88 (s, 3H), 3.98 (s, 6H), 4.02 (bs, 2H), 7.00 (s, 2H). MS (ESI): $[M]^+ = 377.6$. Anal. calcd for $C_{18}H_{23}N_3O_4S$: C, 57.28; H, 6.14; N, 11.13; found: C, 57.02; H, 5.98; N, 11.01.

*5.1.6.5. (4-Amino-2-morpholin-4-yl-1,3-thiazol-5-yl)(3,4,5-trimethoxyphenyl)methanone (**3h**).* Following the general procedure, using morpholine (180 μL) and 2-bromo-1-(3,4,5-trimethoxyphenyl)ethanone (1156 mg), compound **3h** was isolated as a yellow solid. Yield 68%, mp 186–188 °C ^{1}H NMR ($CDCl_3$) δ: 3.56 (t, $J = 5.0$ Hz, 4H), 3.76 (t, $J = 5.0$ Hz, 4H), 3.86 (s, 3H), 3.89 (s, 6H), 4.14 (bs, 2H), 7.00 (s, 2H). MS (ESI): $[M]^+ = 379.8$. Anal. calcd for $C_{17}H_{21}N_3O_5S$: C, 53.81; H, 5.58; N, 11.07; found: C, 53.64; H, 5.38; N, 10.91.

*5.1.6.6. (4-Amino-2-pyrrolidin-1-yl-1,3-thiazol-5-yl)(3,4-dimethoxyphenyl)methanone (**3i**).* Following the general procedure, using pyrrolidine (170 μL) and 2-bromo-1-(4,5-dimethoxyphenyl)ethanone (1040 mg), compound **3i** was isolated as a yellow solid. Yield 75%, mp 218–220 °C ^{1}H NMR ($CDCl_3$) δ: 2.06 (m, 4H), 3.44 (m, 6H), 3.92 (s, 3H), 3.94 (s, 3H), 6.85 (d, $J = 8.0$ Hz, 2H), 7.36 (s, 1H), 7.38 (d, $J = 8.0$ Hz, 2H),. MS (ESI): $[M]^+ = 333.5$. Anal. calcd for $C_{16}H_{19}N_3O_3S$: C, 57.64; H, 5.74; N, 12.60; found: C, 57.51; H, 5.52; N, 12.48.

*5.1.6.7. (4-Amino-2-pyrrolidin-1-yl-1,3-thiazol-5-yl)(4-methoxyphenyl) methanone (**3j**).* Following the general procedure, using pyrrolidine (170 μL) and 2-bromo-1-(4-methoxyphenyl)ethanone (920 mg), compound **3j** was isolated as a yellow solid. Yield 74%, mp 203–205 °C ^{1}H NMR ($CDCl_3$) δ: 2.05 (t, $J = 6.6$ Hz, 4H), 3.48 (m, 6H), 3.85 (s, 3H), 6.90 (d, $J = 8.4$ Hz, 2H), 7.74 (d, $J = 8.4$ Hz, 2H). MS (ESI): $[M]^+ = 303.5$. Anal. calcd for $C_{15}H_{17}N_3O_2S$: C, 59.38; H, 5.65; N, 13.85; found: C, 59.13; H, 5.44; N, 13.71.

*5.1.6.8. (4-Amino-2-pyrrolidin-1-yl-1,3-thiazol-5-yl)(3-methoxyphenyl) methanone (**3k**).* Following the general procedure, using pyrrolidine (170 μL) and 2-bromo-1-(3-methoxyphenyl)ethanone (920 mg), compound **3k** was isolated as a yellow solid. Yield 69%, mp 180–182 °C ^{1}H NMR ($CDCl_3$) δ: 2.06 (t, $J = 6.6$ Hz, 4H), 3.46 (m, 6H), 3.85 (s, 3H), 6.99 (m, 1H), 7.32 (m, 3H). MS (ESI): $[M]^+ = 303.4$. Anal. calcd for $C_{15}H_{17}N_3O_2S$: C, 59.38; H, 5.65; N, 13.85; found: C, 59.21; H, 5.48; N, 13.74.

*5.1.6.9. (4-Amino-2-(pyrrolidin-1-yl)thiazol-5-yl)(2-methoxyphenyl) methanone (**3l**).* Following the general procedure, using pyrrolidine (170 μL) and 2-bromo-1-(2-methoxyphenyl)ethanone (920 mg), compound **3l** was isolated as a yellow solid. Yield 74%, mp 204–206 °C

^{1}H NMR ($CDCl_3$) δ: 2.02 (t, J = 6.6 Hz, 4H), 3.43 (m, 6H), 3.84 (s, 3H), 6.92 (t, J = 8.6 Hz, 2H), 7.35 (m, 2H). MS (ESI): $[M]^+ = 303.3$. Anal. calcd for $C_{15}H_{17}N_3O_2S$: C, 59.38; H, 5.65; N, 13.85; found: C, 59.18; H, 5.38; N, 13.70.

*5.1.6.10. (4-Amino-2-pyrrolidin-1-yl-1,3-thiazol-5-yl)(4-chlorophenyl) methanone (**3m**).* Following the general procedure, using pyrrolidine (170 μL) and 2-bromo-1-(4-chlorophenyl)ethanone (934 mg), compound **3m** was isolated as a yellow solid. Yield 68%, mp 206–208 °C ^{1}H NMR ($CDCl_3$) δ: 2.06 (t, J = 6.6 Hz, 4H), 3.49 (m, 6H), 7.36 (d, J = 8.4 Hz, 2H), 7.69 (d, J = 8.4 Hz, 2H). MS (ESI): $[M]^+ = 307.8$. Anal. calcd for $C_{14}H_{14}ClN_3OS$: C, 54.63; H, 4.58; N, 13.65; found: C, 54.38; H, 4.41; N, 13.52.

*5.1.6.11. (4-Amino-2-pyrrolidin-1-yl-1,3-thiazol-5-yl)(4-bromophenyl) methanone (**3n**).* Following the general procedure, using pyrrolidine (170 μL) and 2-bromo-1-(4-bomophenyl)ethanone (1112 mg), compound **3n** was isolated as a yellow solid. Yield 73%, mp 230–232 °C ^{1}H NMR ($CDCl_3$) δ: 2.08 (t, J = 6.6 Hz, 4H), 3.56 (m, 6H), 7.53 (d, J = 8.4 Hz, 2H), 7.60 (d, J = 8.4 Hz, 2H). MS (ESI): $[M]^+ = 352.4$. Anal. calcd for $C_{14}H_{14}BrN_3OS$: C, 47.74; H, 4.01; N, 11.93; found: C, 47.58; H, 3.89; N, 11.74.

*5.1.6.12. (4-Amino-2-pyrrolidin-1-yl-1,3-thiazol-5-yl)(phenyl)methanone (**3o**).* Following the general procedure, using pyrrolidine (170 μL) and 2-bromo-1-phenylethanone (800 mg), compound **3o** was isolated as a yellow solid. Yield 72%, mp 176–178 °C ^{1}H NMR ($CDCl_3$) δ: 2.05 (m, 4H), 3.46 (m, 6H), 7.43 (m, 3H), 7.74 (m, 2H). MS (ESI): $[M]^+ = 273.5$. Anal. calcd for $C_{14}H_{15}N_3OS$: C, 61.51; H, 5.53; N, 15.37; found: C, 61.36; H, 5.37; N, 15.16.

5.2. Biological assays and computational studies

5.2.1. Cell growth inhibitory activity

Murine leukemia L1210, murine mammary carcinoma FM3A, human T-lymphocyte Molt 4 and CEM and human cervix carcinoma (HeLa) cells were suspended at 300,000–500,000 cells/mL of culture medium, and 100 μL of the cell suspension was added to 100 μL of an appropriate dilution of the test compounds in wells of 96-well microtiter plates. After incubation at 37 °C for two days, the cell number was determined using a Coulter counter. The IC50 was defined as the compound concentration required to inhibit cell proliferation by 50%. Data are expressed as the mean ± SE from the dose–response curves of at least three independent experiments.

5.2.2. Effects on tubulin polymerization and on colchicine binding to tubulin

Bovine brain tubulin was purified as described previously [21]. To evaluate the effect of the compounds on tubulin assembly *in vitro* [22], varying concentrations were preincubated with 10 μM tubulin in glutamate buffer at 30 °C and then cooled to 0 °C. After addition of GTP, the mixtures were transferred to 0 °C cuvettes in a recording spectrophotometer and warmed to 30 °C, and the assembly of tubulin was observed turbidimetrically. The IC_{50} was defined as the compound concentration that inhibited the extent of assembly by 50% after a 20 min incubation. The capacity of the test compounds to inhibit colchicine binding to tubulin was measured as described [23], except that the reaction mixtures contained 1 μM tubulin, 5 μM [^{3}H]colchicine and 5 μM test compound.

5.2.3. Molecular modeling

All molecular modeling studies were performed on a MacPro dual 2.66 GHz Xeon running Ubuntu 10. The tubulin structure was downloaded from the PDB data bank (http://www.rcsb.org/ - PDB code: 1SA0) [24]. Hydrogen atoms were added to the protein, using Molecular Operating Environment (MOE) [25], and minimized keeping all the heavy atoms fixed until a RMSD gradient of 0.05 kcal mol^{-1} Å^{-1} was reached. Ligand structures were built with MOE and minimized using the MMFF94x forcefield until a RMSD gradient of 0.05 kcal mol^{-1} Å^{-1} was reached. The docking simulations were performed using PLANTS [26].

5.2.4. Antiproliferative assays on MDR cells

LoVo^{Doxo} is a doxorubicin resistant subclone of LoVo cells and were grown in complete HAM's F12 medium supplemented with doxorubicin (0.1 μg/ml). CEM$^{Vbl-100}$ is a multidrug-resistant line selected against vinblastine. A549-T12 is a non-small cell lung carcinoma cells exhibiting resistance to taxol. They were grown in complete DMEM medium supplemented with taxol (12 nM). Individual wells of a 96-well tissue culture microtiter plate were inoculated with 100 μL of complete medium containing 8×10^3 cells. The plates were incubated at 37 °C in a humidified 5% CO_2 incubator for 18 h prior to the experiments. After medium removal, 100 μL of the drug solution, dissolved in complete medium at different concentrations, was added to each well and incubated at 37 °C for 72 h. Cell viability was assayed by the (3-(4,5-dimethylthiazol-2-yl)-2,5-diphenyl tetrazolium bromide) (MTT) test as described previously [18]. The IC50 was defined as the compound concentration required to inhibit cell proliferation by 50%.

5.2.5. Flow cytometric analysis of cell cycle distribution

For flow cytometric analysis of DNA content, 5×10^5 HeLa cells in exponential growth were treated with different concentrations of the test compounds for 24 and 48 h. After an incubation period, the cells were collected, centrifuged and fixed with ice-cold ethanol (70%). The cells were then treated with lysis buffer containing RNAse A and 0.1% Triton X-100, and then stained with PI. Samples were analyzed on a Cytomic FC500 flow cytometer (Beckman Coulter). DNA histograms were analyzed using MultiCycle® for Windows (Phoenix Flow Systems).

5.2.6. Annexin-V assay

Surface exposure of PS on apoptotic cells was measured by flow cytometry with a Coulter Cytomics FC500 (Beckman Coulter) by adding Annexin-V-FITC to cells according to the manufacturer's instructions (Annexin-V Fluos, Roche Diagnostic). Simultaneously, the cells were stained with PI. Excitation was set at 488 nm, and the emission filters were at 525 nm and 585 nm, for measurement of FTIC and PI fluorescence, respectively.

5.2.7. Assessment of mitochondrial changes

The mitochondrial membrane potential was measured with the lipophilic cation JC-1, while the production of ROS was followed by flow cytometry using the fluorescent dyes HE and H_2DCFDA (the three compounds were from Molecular Probes, USA) as previously described [18]. Briefly, after different times of treatment, the cells were trypsinized, collected by centrifugation and resuspended in Hank's Balanced Salt Solution (HBSS) containing the JC-1 (1 μM), HE (2.5 μM) or H_2DCFDA (0.1 μM). The cells were then incubated for 10 min at 37 °C, centrifuged and resuspended in HBSS and analyzed by flow cytometry.

5.2.8. Caspase-3 assay

Caspase-3 activation in Jurkat cells was evaluated by flow cytometry using a human active caspase-3 fragment antibody conjugated with FITC (BD Pharmingen). Briefly, after different incubation times in the presence of test compounds, the cells were collected by centrifugation and resuspended in Cytofix™ (BD Pharmingen) buffer for 20 min, washed with Perm/Wash™ (BD

Pharmingen) and then incubated for 30 min with the antibody. After this period, cells were washed and analyzed by flow cytometry. Results are expressed as percentage of caspase-3 active fragment positive cells.

5.2.9. Western blot analysis

HeLa cells were incubated in the presence of test compounds and, after different times, were collected, centrifuged and washed two times with ice cold PBS. The pellet was then resuspended in lysis buffer. After the cells were lysed on ice for 30 min, lysates were centrifuged at 15,000× *g* at 4 °C for 10 min. The protein concentration in the supernatant was determined using BCA protein assay reagents (Pierce, Italy). Equal amounts of protein (20 μg) were resolved using sodium dodecyl sulfate polyacrylamide gel electrophoresis (SDS-PAGE) (7.5–15% acrylamide gels) and transferred to PVDF Hybond-p membrane (GE Healthcare). Membranes were blocked with I-block (Tropix) the membrane being gently rotated overnight at 4 °C. Membranes were then incubated with primary antibodies against Bcl-2, Bax, cleaved PARP, (all rabbit, 1:1000, Cell Signaling), cyclin B, p-cdc2^{Tyr15}, cdc25c, or β-actin (mouse, 1:10,000, Sigma) for 2 h at room temperature. Membranes were next incubated with peroxidase-labeled goat anti-rabbit IgG (1:100,000, Sigma) or peroxidase-labeled goat anti-mouse IgG (1:100,000, Sigma) for 60 min. All membranes were visualized using ECL Advance (GE Healthcare) and exposed to Hyperfilm MP (GE Healthcare). To ensure equal protein loading, each membrane was stripped and reprobed with anti-β-actin antibody.

5.2.10. Antitumor activity in vivo

Four weeks old, Female BALB/c-nu nude mice (15–18 g) were obtained from Shanghai SLAC Laboratory Animal Co., Ltd. (Shanghai, China). The animals were maintained under specific pathogen-free conditions with food and water supplied ad libitum in the Zhejiang University of Traditional Chinese Medicine Laboratory Animal Center. Human colon adenocarcinoma HT-29 cells in logarithmic growth phase were suspended in fetal bovine serum-free RPMI 1640 at 1×10^7cells/mL and inoculated in 0.2 mL into the hypodermis of the pars dorsalis of each mouse. Once the HT-29 xenografts reached a size of ~300 mm^3, eighteen mice were randomly assigned either to the control group or one of two treatment groups: Compound **3f** and **CA-4** were prepared in DMSO and injected intraperitoneally at 0.01 mL/g body weight to give a dose of 100 mg/kg. The drugs or vehicle were administered three times a week for one week. After completing the treatment schedule (23 days), except when death occurred earlier, tumor-bearing mice were euthanized. Tumor volume was calculated by the formula: $V = \times (L \times W^2)/2$, where L is the length and W is the width of the tumor nodules measured by vernier caliper. The study was approved by the Institutional Animal Ethical Committee of the Second Affiliated Hospital, School of Medicine, Zhejiang University (PRC).

5.2.11. Statistical analysis

Unless indicated differently, the results are presented as mean ± S.E.M. The differences between different treatments were analyzed using the two-sided Student's *t* test. *P* values lower than 0.05 were considered significant.

Acknowledgments

Financial support was provided by GOA (Krediet no. 10/014) of the K.U.Leuven. The authors would like to thank Mrs. Lizette van Berckelaer and Dr. Alberto Casolari for technical assistance.

Appendix. Supplementary data

Supplementary data associated with this article can be found, in the online version, at doi:10.1016/j.ejmech.2011.10.013.

References

[1] A.L. Risinger, F.J. Giles, S.L. Mooberry, Microtubule dynamics as a target in oncology, Cancer Treat. Rev. 35 (2008) 255–261.
[2] S. Honore, E. Pasquier, D. Braguer, Understanding microtubule dynamics for improved cancer therapy, Cell. Mol. Life Sci. 62 (2005) 3039–3056.
[3] G.R. Pettit, S.B. Singh, E. Hamel, C.M. Lin, D.S. Alberts, D. Garcia-Kendall, Isolation and structure of the strong cell growth and tubulin inhibitor combretastatin A-4, Experientia 45 (1989) 209–211.
[4] C.M. Lin, H.H. Ho, G.R. Pettit, E. Hamel, Antimitotic natural products combretastatin A-4 and combretastatin A-2: studies on the mechanism of their inhibition of the binding of colchicine to tubulin, Biochemistry 28 (1989) 6984–6991.
[5] A. Chaudari, S.N. Pandeya, P. Kumar, P.P. Sharma, S. Gupta, N. Soni, K.K. Verma, G. Bhardwaj, Combretastain A-4 analogues as anticancer agents, Mini Rev. Med. Chem. 12 (2007) 1186–1205.
[6] R. Romagnoli, P.G. Baraldi, M.D. Carrion, O. Cruz-Lopez, C. Lopez-Cara, G. Basso, G. Viola, M. Khedr, J. Balzarini, S. Mahboobi, A. Sellmer, A. Brancale, E. Hamel, 2-Arylamino-4-Amino-5-Aroylthiazoles. "One-Pot" synthesis and biological evaluation of a new class of inhibitors of tubulin polymerization, J. Med. Chem. 52 (2009) 5551–5555.
[7] K. Gaukroger, J.A. Hadfield, N.J. Lawrence, S. Nlan, A.T. McGown, Structural requirements for the interaction of combretastatins with tubulin: how important is the trimethoxy unit? Org. Biomol. Chem. 1 (2003) 3033–3037.
[8] (a) D. Thomae, E. Perspicace, S. Hesse, G. Kirsch, P. Seck, Synthesis of substituted [1,3]thiazolo[4,5-d][1,2.3]triazines, Tetrahedron 64 (2008) 9306–9314;
(b) D. Thomae, E. Perspicace, Z. Xu, D. Henryon, S. Schneider, S. Hesse, G. Kirsch, P. Seck, One-pot synthesis of new 2,4,5-trisubstituted 1,3-thiazoles and 1,3-selenazoles, Tetrahedron 65 (2009) 2982–2988.
[9] G. Szakács, J.K. Paterson, J.A. Ludwig, C. Booth-Genthe, M.M. Gottesman, Targeting multidrug resistance in cancer, Nat. Rev. Drug Discov. 5 (2006) 219–234.
[10] B.C. Baguley, Multidrug resistance mechanism in cancer, Mol. Biotechnol. 46 (2010) 308–316.
[11] M. Dupuis, M. Flego, A. Molinari, M. Cianfriglia, Saquinavir induces stable and functional expression of the multidrug transporter P-glycoprotein in human CD4 T-lymphoblastoid CEM rev cells, HIV Med. 4 (2003) 338–345.
[12] G. Toffoli, A. Viel, I. Tuimoto, G. Bisconti, G. Rossi, M. Baoiocchi, Pleiotropic-resistant phenotype is a multifactorial phenomenon in human colon carcinoma cell lines, Br. J. Cancer 63 (1991) 51–56.
[13] L.A. Martello, P. Verdier-Pinard, H.J. Shen, L. He, K. Torres, G.A. Orr, S.B. Horwitz, Elevated level of microtubule destabilizing factors in a taxol-resistant/ dependent A549 cell line with an alpha-tubulin mutation, Cancer Res. 63 (2003) 448–454.
[14] F. Mollinedo, C. Gajate, Microtubules, microtubule-interfering agents and apoptosis, Apoptosis 8 (2003) 413–450.
[15] I. Vermes, C. Haanen, H. Steffens-Nakken, C. Reutelingsperger, A novel assay for apoptosis. Flow cytometric detection of phosphatidylserine expression on early apoptotic cells using fluorescein labelled annexin V, J. Immunol. Methods 184 (1995) 39–51.
[16] S.J. Martin, C.P. Reutelingsperger, A.J. Mc Gahon, J.A. Rader, R.C. van Schie, D.M. Laface, D.R. Green, Early redistribution of plasma membrane phosphatidylserine is a general feature of apoptosis regardless of the initiating stimulus: inhibition by overexpression of Bcl-2 and Abl, J. Exp. Med. 182 (1995) 1545–1556.
[17] (a) J.D. Ly, D.R. Grubb, A. Lawen, The mitochondrial membrane potential ($\Delta\psi_m$) in apoptosis: an update, Apoptosis 3 (2003) 115–128;
(b) D.R. Green, G. Kroemer, The pathophysiology of mitochondrial cell death, Science 305 (2005) 626–629.
[18] G. Viola, E. Fortunato, L. Cecconet, L. Del Giudice, F. Dall'Acqua, G. Basso, Central role of mitochondria and p53 in PUVA-induced apoptosis in human keratinocytes cell line NCTC-2544, Toxicol. Appl. Pharm. 227 (2008) 84–96.
[19] (a) G. Rothe, G. Valet, Flow cytometric analysis of respiratory burst activity in phagocytes with hydroethidine and 2′,7′-dichlorofluorescein, J. Leukoc. Biol. 47 (1990) 440–448;
(b) J. Cai, D.P. Jones, Superoxide in apoptosis. Mitochondrial generation triggered by cytochrome *c* loss, J. Biol. Chem. 273 (1998) 11401–11404;
(c) H. Nohl, L. Gille, K. Staniek, Intracellular generation of reactive oxygen species by mitochondria, Biochem. Pharmacol. 69 (2005) 719–723.
[20] (a) R.M. Kluck, E. Bossy-Wetzel, D.R. Green, The release of cytochrome c from mitochondria: a primary site for Bcl-2 regulation of apoptosis, Science 275 (1997) 1132–1136;
(b) C.M. Knudson, S.J. Korsmeyer, Bcl-2 and Bax function independently to regulate cell death, Nat. Genet. 16 (1997) 358–363.

[21] E. Hamel, C.M. Lin, Separation of active tubulin and microtubule-associated proteins by ultracentrifugation, and isolation of a component causing the formation of microtubule bundles, Biochemistry 23 (1984) 4173–4184.
[22] E. Hamel, Evaluation of antimitotic agents by quantitative comparisons of their effects on the polymerization of purified tubulin, Cell Biochem. Biophys. 38 (2003) 1–21.
[23] P. Verdier-Pinard, J.-Y. Lai, H.-D. Yoo, J. Yu, B. Marquez, D.G. Nagle, M. Nambu, J.D. White, J.R. Falck, W.H. Gerwick, B.W. Day, E. Hamel, Structure-activity analysis of the interaction of curacin A, the potent colchicine site antimitotic agent, with tubulin and effects of analogs on the growth of MCF-7 breast cancer cells, Mol. Pharmacol. 53 (1998) 62–67.
[24] R.B.G. Ravelli, B. Gigant, P.A. Curmi, I. Jourdain, S. Lachkar, A. Sobel, M. Knossow, Insight into tubulin regulation from a complex with colchicine and a stathmin-like domain, Nature 428 (2004) 198–202.
[25] Molecular Operating Environment (MOE 2010.10). Chemical Computing Group, Inc. Montreal, Quebec, Canada. http://www.chemcomp.com.
[26] O. Korb, T. Stützle, T.E. Exner, PLANTS: application of ant colony optimization to structure-based drug design. in: M. Dorigo, L.M. Gambardella, M. Birattari, A. Martinoli, R. Poli, T. Sttzle (Eds.), Ant Colony Optimization and Swarm Intelligence, 5th International Workshop, ANTS 2006, Brussels, Belgium. Springer, Berlin, Sep 4–7, 2006, pp. 247–258 2006; LNCS 4150.